Coexistence of antiferromagnetic and spin-glass behaviour in $U_3Rh_3Sb_4$

2005 J. Phys.: Condens. Matter 17 3597

(http://iopscience.iop.org/0953-8984/17/23/012)

INSTITUTE OF PHYSICS PUBLISHING JOURNAL OF PHYSICS: CONDENSED MATTER

J. Phys.: Condens. Matter **17** (2005) 3597–3609 doi:10.1088/0953-8984/17/23/012

Coexistence of antiferromagnetic and spin-glass behaviour in $U_3Rh_3Sb_4$

V H Tran, Z Bukowski, J Stępień-Damm, A J Zaleski, D Badurski, R Gorzelniak, Cz Sułkowski and R Troć

W Trzebiatowski Institute of Low Temperature and Structure Research, Polish Academy of Sciences, PO Box 1410, P-50-950 Wrocław, Poland

Received 20 December 2004, in final form 7 April 2005
Published 27 May 2005
Online at stacks.iop.org/JPhysCM/17/3597

Abstract

We report on single-crystal growth, crystal structural determination and magnetic, electrical resistivity and thermoelectric power measurements performed on a set of single crystals of $U_3Rh_3Sb_4$. The compound crystallizes in the cubic $Y_3Au_3Sb_4$-type structure. The ac susceptibility and dc magnetization both indicate that the compound undergoes a transition into a spin-glass state below 14.7 K. The resistivity shows a broad minimum at 30 K. The thermoelectric power is negative in the whole temperature range studied and exhibits an enhanced value of $-32\ \mu V\ K^{-1}$ at room temperature.

(Some figures in this article are in colour only in the electronic version)

1. Introduction

The $U_3T_3M_4$ (T is a transition metal, M = Sn or Sb) series of intermetallic compounds crystallizes in the cubic structure of $Y_3Au_3Sb_4$ type [1–3]. Some of these intermetallics exhibit interesting physical properties; for example, the stannides with T = Cu and Au were reported to show a heavy-fermion behaviour while the antimonides with T = Ni, Pd and Pt were found to be semiconductors [3, 4]. Moreover, $U_3Pt_3Sb_4$ was reported to have a hybridization gap [5], similar to that observed in a classical heavy-fermion semiconductor such as $Ce_3Pt_3Sb_4$ [6]. Amongst ten $U_3T_3M_4$-type compounds known up to now, only $U_3Cu_3Sn_4$ was found to have an antiferromagnetic ground state [4, 7]. Three others, $U_3Co_3Sb_4$, $U_3Cu_3Sb_4$ [2, 4, 7] and $U_3Rh_3Sb_4$ [8], are ferromagnets. It has also been reported that a polycrystalline sample of the latter compound contains some impurities but it exhibits the highest Curie temperature of 105 K [8]. In this study we report on the single-crystal growth and crystal structure refinement of $U_3Rh_3Sb_4$ based on single-crystal x-ray data at room temperature. We report also on the ac susceptibility, dc magnetization, electrical resistivity and thermoelectric power measurements made on single crystals of this compound. In contrast with the reported data in the literature, $U_3Rh_3Sb_4$ is considered here to exhibit a coexistence of antiferromagnetic short range and a spin-glass order below 14.7 K. We will discuss the possible mechanisms leading to the spin-glass behaviour in $U_3Rh_3Sb_4$.

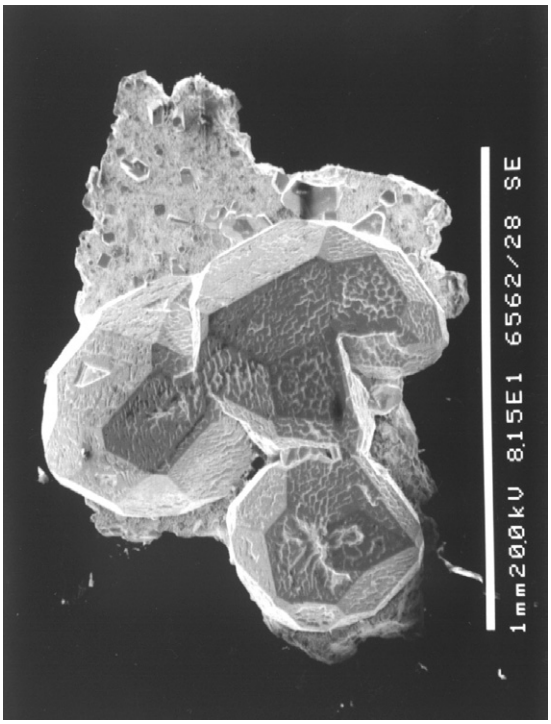

Figure 1. SEM micrograph of a set of single crystals of $U_3Rh_3Sb_4$.

2. Experimental details

Some amounts of small single crystals of $U_3Rh_3Sb_4$ were grown using an indium-flux method [11]. Stoichiometric amounts of uranium (purity 99.98%), rhodium and antimony (purity 99.99%) in the atomic ratio of 3:3:4 were arc-melted together in a pure argon atmosphere. The obtained sample was powdered and mixed with In in a 1:10 weight ratio. The mixture was placed in an alumina crucible, sealed in an evacuated silica tube and heated up to 1150 °C for 10 h, then followed by slow cooling (3 °C h^{-1}) down to 450 °C. The flux was removed by decanting. Thin In film on the surface of the crystals was eliminated by etching with a solution of citric and nitric acids. A large number of small single crystals of $U_3Rh_3Sb_4$ were formed, being cube shaped with a typical dimension of $0.5 \times 0.5 \times 0.5$ mm^3 (figure 1). The quality of single crystals was checked with the Laue method, an optical microscope, a scanning Philips 515 electron microscope and an energy dispersive x-ray (EDX) analysis. The analysis showed a good quality of the crystals. The compositional U:Rh:Sb ratio was determined to be 27:28:45, in fairly good agreement with the expected ratio of 30:30:40. The phase purity of crystals was checked by powder x-ray diffraction of crushed single crystals. The crystal structure was refined using SHELXL-97 (full-matrix least squares on F^2) [12]. The single-crystal x-ray diffraction data were collected with an Xcalibur-CCD diffractometer (Mo Kα radiation). The dc magnetization measurements were performed in magnetic fields up to 5 T with a SQUID magnetometer (Quantum Design) in the temperature range 2–400 K. The measurements were performed on a sample with the field cooled (FC) and zero-field cooled (ZFC) modes. The ac magnetic susceptibility measurements were carried out within the frequency range 100–10 000 Hz, utilizing a susceptometer (Maglab, Oxford Instruments).

Table 1. Crystallographic data and structure refinement for $U_3Rh_3Sb_4$.

Formula weight	1509.82
Wavelength	0.710 73 Å
Crystal system, space group	Cubic, $I\bar{4}3d$
Unit cell dimensions	$a = 9.501(1)$ Å
Z, Calculated density	4, 11.693 Mg m^{-3}
Absorption coefficient	74.320 mm^{-1}
$F(000)$	2460
Theta range for data collection	5.26°–39.24°
Limiting indices	$-16 \leqslant h \leqslant 11$, $-15 \leqslant k \leqslant 16$, $-12 \leqslant l \leqslant 16$
Reflections collected/unique	5186/428 [R(int) = 0.1406]
Completeness to theta	=39.14 99.6%
Refinement method	Full-matrix least squares on F^2
Data/restraints/parameters	428/0/9
Goodness-of-fit on F^2	1.051
Final R indices [$I > 2$sigma(I)]	$R1 = 0.0462$, $wR2 = 0.1270$
R indices (all data)	$R1 = 0.0472$, $wR2 = 0.1281$
Extinction coefficient	0.0013(2)
Largest diff. peak and hole	4.430 and −10.499 e Å^{-3}

Table 2. Atomic coordinates ($\times 10^4$) and equivalent isotropic displacement parameters ($A^2 \times 10^3$) for $U_3Rh_3Sb_4$. $U(eq)$ is defined as one third of the trace of the orthogonalized U_{ij} tensor. Anisotropic displacement parameters (Å^2 × 10^3) for $U_3Rh_3Sb_4$. The anisotropic displacement factor exponent takes the form $2\pi^2[h^2a^2U_{11} + \cdots + 2hka^*b^*U_{12}]$.

Atoms	x	z	z	$U(eq)$	U_{11}	U_{22}	U_{33}
U	3750	0	2500	3(1)	5(1)	2(1)	2(1)
Rh	8750	0	2500	8(1)	8(1)	8(1)	7(1)
Sb	1653	0	0	4(1)	4(1)	4(1)	4(1)

For the magnetic measurements, a set of single crystals was packed into a plastic sample holder, for which a diamagnetic correction has been taken into account. The crystals under the applied magnetic field were able to be oriented along the easy magnetization axis. The electrical resistivity ρ was measured in the range 4.2–300 K employing a conventional dc four-point technique with a current of 10 mA along the [100] direction. The thermoelectric power, S, was measured applying a differential method between 7 and 300 K.

3. Results and analysis

3.1. Single-crystal x-ray diffraction

The powder x-ray diffraction pattern of crushed single crystals of $U_3Rh_3Sb_4$ has revealed the sample to be essentially a single phase of the cubic $Y_3Au_3Sb_4$-type structure with the lattice parameter $a = 9.500(3)$ Å. Moreover, the x-ray analysis of a selected crystal yields a similar value of the lattice parameter, 9.501(1) Å. It turns out that the value of the lattice parameter of our sample is much smaller than that reported earlier in the literature (9.531 Å) [8]. This difference may be caused by a slightly different transition metal composition in both these considered materials. In particular, some vacancies in the position of the transition metal for the $U_3T_3M_4$-type ternaries are possible [8]. In tables 1, 2 we give all the relevant details concerning the x-ray data collected at room temperature, i.e., the atomic positions and

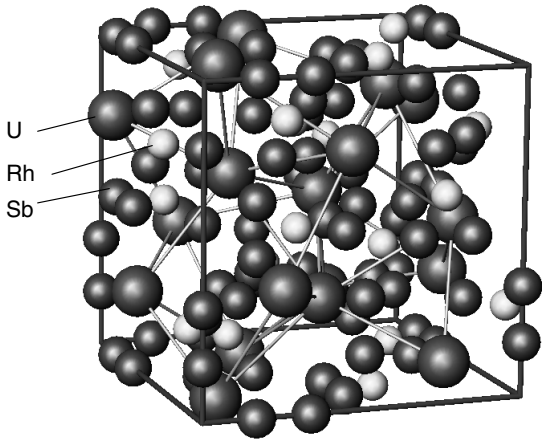

Figure 2. Crystal structure of $U_3Rh_3Sb_4$ with the cubic $Y_3Au_3Sb_4$-type symmetry.

anisotropic displacement parameters. In accordance with the EDX data, the deficit of the Rh or Sb atoms in their crystallographic positions has not been observed within the limits of the experimental error by the single-crystal x-ray refinements (less than 3 at.%). On the other hand, the observation of a relatively large value of the anisotropic displacement parameter for the Rh atoms compared to those of U and Sb (table 2) signals that some vacancy in the 12(b) position is quite possible. In figure 2 we show the crystal structure of $U_3Rh_3Sb_4$. The unit cell contains 12 uranium, 12 rhodium and 16 antimony ions. Inspecting the structure one can distinguish six equivalent sublattices of uranium ions. However, detailed analysis of the crystal and magnetic structures given in [9, 10] proved that two or three different uranium sublattices are possible.

3.2. ac magnetic susceptibility

Figure 3 displays the temperature dependences of the magnetic ac susceptibility of $U_3Rh_3Sb_4$ at three selected frequencies, $\omega/2\pi = 100$, 1000 and 10 000 Hz. As seen in the figure, both the real (χ') and the imaginary (χ'') components exhibit pronounced maxima near 15 K. The amplitudes and positions of these maxima depend on the frequency of the applied magnetic field, which often characterizes a spin-glass-like state being formed at low temperatures. However, for a classical spin-glass behaviour one should observe a cusplike maximum in the temperature dependence of the real part of the susceptibility at a characteristic freezing temperature T_f and a sudden upturn in the imaginary part of the susceptibility at a temperature slightly above T_f [13]. For $U_3Rh_3Sb_4$, however, neither a cusplike maximum in $\chi'(T)$ nor a sudden upturn in $\chi''(T)$ was observed. Indeed, the $\chi'(T)$ curve displays rather a broad maximum, while the $\chi''(T)$ curve has the maximum of a Lorentzian-type shape. This suggests that if $U_3Rh_3Sb_4$ were a spin glass then it would not be a simple spin glass and the $\chi'(T)$ maximum may no longer yield the freezing temperature. Following Goldfarb *et al* [14], we define T_f of $U_3Rh_3Sb_4$ by the peak position of the $\chi''(T)$ curve. At a frequency of 100 Hz, T_f amounts to 14.7 K and increases with the applied frequency (see figure 3). The frequency sensitivity of T_f is obtained from the expression: $\Delta T_f / T_f \Delta \log \varpi = 0.06$. This value is much larger than those of metallic glasses, e.g., CuMn (0.007) and AuFe (0.01) [15], but comparable to the value reported for an insulator spin glass $Eu_{0.6}Sr_{0.4}S$ (0.05) [16].

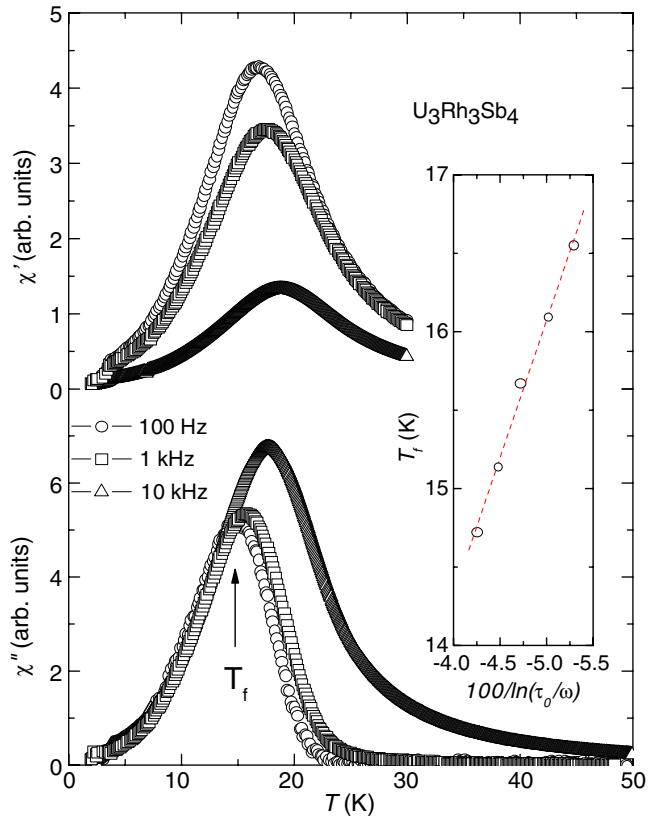

Figure 3. Temperature dependence of the ac magnetic susceptibility of single crystals of $U_3Rh_3Sb_4$ measured at different frequencies. The inset illustrates the Vogel–Fulcher law.

In order to describe the time-dependent effects in spin glasses one uses the Vogel–Fulcher law [15, 17]:

$$\tau = 1/\omega = \tau_0 \exp\left[\frac{E_a}{k_B(T_f - T_0)}\right] \tag{1}$$

where τ_0 is an intrinsic relaxation time, E_a is an activation energy and T_0 is the spin-glass temperature. Assuming $\tau_0 = 10^{-13}$ s we could fit the T_f versus frequency data to equation (1) with $T_0 = 7.3$ K and $E_a/k_B = 175$ K (inset of figure 3).

3.3. Magnetic susceptibility and magnetization

dc magnetic susceptibility was calculated from the relation $\chi = M/\mu_0 H$. For $U_3Rh_3Sb_4$ we observe that χ below 200 K depends strongly on the applied magnetic strength fields strengths. This behaviour is due to some magnetic correlations between magnetic centres. In figure 4(a) we show the temperature dependence of the reciprocal ZFC magnetic susceptibility measured at a large field of 5 T, where the correlation is expected to stabilize. It appears that the $\chi(T)$ dependence at temperatures above 200 K tends to follow the Curie–Weiss law. From the fit of the experimental data to this law in the temperature range 250–400 K we obtained the effective magnetic moment $\mu_{eff} = 3.2(1)\ \mu_B$ and the paramagnetic Curie temperature $\Theta_p = -110(2)$ K. Apparently, the μ_{eff} value found for $U_3Rh_3Sb_4$ is a little smaller than those reported for the

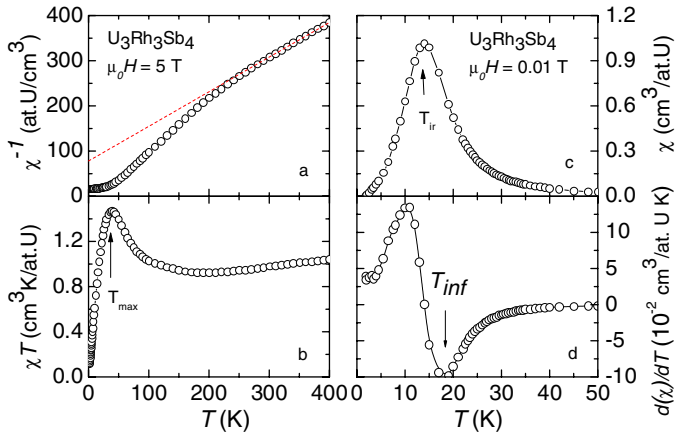

Figure 4. (a) Temperature dependence of the ZFC magnetic susceptibility of single crystals of $U_3Rh_3Sb_4$ measured at a field of 5 T. The dashed line is a Curie–Weiss fit. (b) The product χT versus temperature. (c) The ZFC susceptibility measured at 0.01 T as a function of temperature. (d) The temperature derivative of the susceptibility at 0.01 T as a function of temperature.

other $U_3T_3Sb_4$-type (T = Ni, Cu, Pd and Pt) compounds (3.4–3.7 μ_B) [4]. This fact may reflect a more itinerant character of the 5f electrons in this Rh-based compound as a result of a stronger hybridization between the 5f and spd valence electrons of the Rh/Sb atoms. In figure 4(b) we show the product χT as a function of temperature. With decreasing temperature from 400 K, this product firstly slightly decreases. Such a temperature variation of the χT versus T curve is expected for the case of an antiferromagnetic coupling between the uranium ions. This, in turn, is in consistence with the negative value of Θ_p. As T is further decreased from 160 K the product χT starts to increase until it reaches its maximum value at $T_{max} = 36$ K. The observed increase in χT below 160 K indicates that a ferromagnetic (F) correlation of the uranium ions first becomes dominant in this temperature range and then below T_{max} an antiferromagnetic (AF) coupling starts to dominate. The competition between the F and AF interactions presumably leads to a spin-glass behaviour at low temperatures. In addition to the spin-glass phenomenon, accompanied by the maximum in the ZFC dc susceptibility at the irreversible temperature T_{ir} (figure 4(c)), we suspect from a minimum in the $d(\chi)/dT$ versus T curve (figure 4(d)) denoting $T_{inf} \approx 17$ K, that some additional phase transition, probably of ferromagnetic origin, sets in in this compound below this temperature.

The low temperature magnetization data taken at several magnetic fields are shown in figure 5. Clearly, all the ZFC-type curves are characterized by a rapid drop in the ZFC magnetization at T_{ir} and by the inflexion point at T_{inf}. For the sake of clarity we have marked the positions of T_{ir} and T_{inf} by arrows only for the 3 T magnetization curve. In order to find any relationship between the applied field and T_{inf} we have plotted in figure 5(b) a preliminary H–T diagram for $U_3Rh_3Sb_4$, in which it is evident that the applied field shifts T_{inf} to higher values. Such a behaviour is typical of a ferromagnetic transition. We have tried to fit the $H(T_{inf})$ dependence to a power law $H = H_0^{inf}(T/T_{C,0} - 1)^n$, where $H_0^{inf} = 3.74(3)$ T, $n = 1.65(5)$ and $T_{C,0} = 16.9(0.2)$ K. In the case of a magnetic phase transition, the exponent n is related to the critical exponents γ and β as $n = \gamma + \beta$ [18]. Both the γ and β exponents may be calculated from theory [19]. In the 3D systems, the mean field theory gives $\beta = 0.5$ and $\gamma = 1$, while the classical Heisenberg model yields $\beta = 0.38$ and $\gamma = 1.375$ [19]. It appears that our experimental values are then located between these theoretical values.

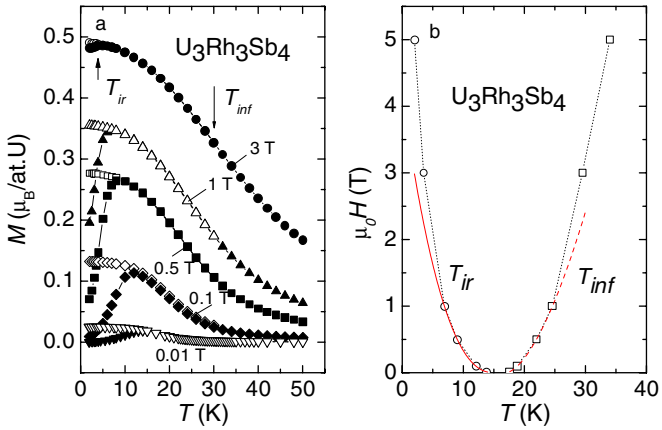

Figure 5. (a) Temperature dependences of the ZFC (closed symbols) and FC (open symbols) magnetizations measured at several fields; (b) the field dependences of T_{ir} and T_{inf}. The dotted lines are guides for the eyes. The solid and dashed lines are fits (see text).

Upon warming the field-cooled samples from 2 to 50 K, the FC $M(T)$ curves do not exhibit any maximum. Thus, in comparison with the ZFC magnetization data, we observe an irreversibility below T_{ir}. For $U_3Rh_3Sb_4$ such an irreversibility persists in fields even up to 5 T. In turn, such a behaviour supports the existence of the spin-glass state in $U_3Rh_3Sb_4$. We have found that the field dependence of T_{ir} follows the equation $H = H_0^{ir}(T_{ir,0}/T - 1)^a$. Figure 5(b) displays both the experimental (open circles) and fitted (solid line) H versus T_{ir} data where in low magnetic fields $H_0^{ir} = 4.16(3)$, $T_{ir,0} = 14.8(3)$ K and $a = 2.34(2)$. The value of $T_{ir,0}$ agrees well with the freezing temperature T_f deduced from the ac susceptibility taken at a frequency of 100 Hz. On the other hand, the exponent a is considerably larger than that of the mean-field value of 3/2 predicted by Almeida and Thouless for spin-glass materials [20]. Note that a similar magnitude of a (=2.35) can be deduced, e.g., for the AlGd system [21].

In figure 6 we show the magnetization isotherms measured below 10 K. For the sake of clarity, the data for increasing (open circles) and decreasing (closed circles) magnetic field are only shown for the 2 K magnetization curves. All isotherms below 10 K display a similar dependence and may be characterized by several features. The most prominent observation is a metamagnetic-like transition at a critical field H_{cr}. For the 2 K magnetization curve, H_{cr} amounts to about 1.1 T. At a larger field of 5 T the magnetization achieves a considerable value of 0.55 μ_B, but there is no saturation effect observed, even at a magnetic field of 9 T applied in the Oxford susceptometer (not shown here). Furthermore, a sizable hysteresis loop with the remanence magnetization M_r and a small coercivity field H_{coe} were found. The magnetization at 2 K may be represented by the values of 0.23 μ_B and of 0.75 T for M_r and H_{coe}, respectively. This means that the AF phase or at least some of the magnetic ions with the AF coupling undergoes the ferro(ferri) phase transition. In the inset of figure 6 we show the field derivative of the magnetization for several selected temperatures. For $T < 10$ K all the $M(H)$ curves have an antiferromagnetic characteristic, showing a shift of H_{cr} down to lower values when T is increased. Assuming a power law for the $H_{cr}(T)$ dependence, we found that the critical field is shifted with temperature following the equation $H_{cr} = 2 * (1 - T/14.7)^{9/2}$.

The magnetization taken between 12 and 30 K vary in a manner typical of either a weak ferromagnet or a material with a strong ferromagnetic correlation. A similar magnetization curve was reported for a ferromagnet $U_3Co_3Sb_4$ [7]. However, the ferromagnetic ground state of this compound was not confirmed by the NMR and NQR studies [22].

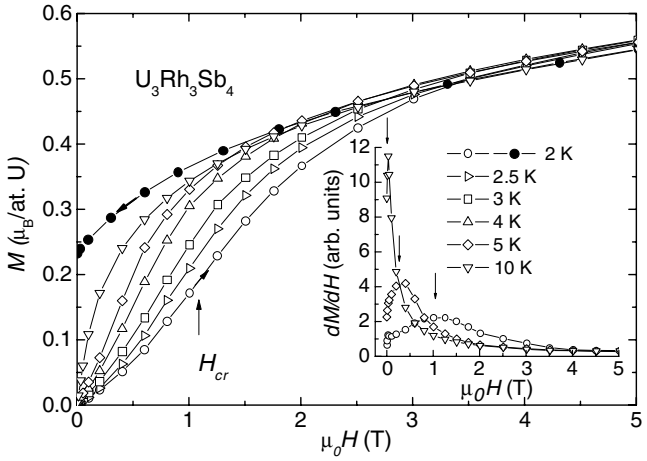

Figure 6. Magnetization of single crystals of $U_3Rh_3Sb_4$ measured at several temperatures below 10 K. The inset shows the field derivative of the magnetization taken for 2, 5 and 10 K. The arrows illustrate the change of H_{cr} with the applied fields.

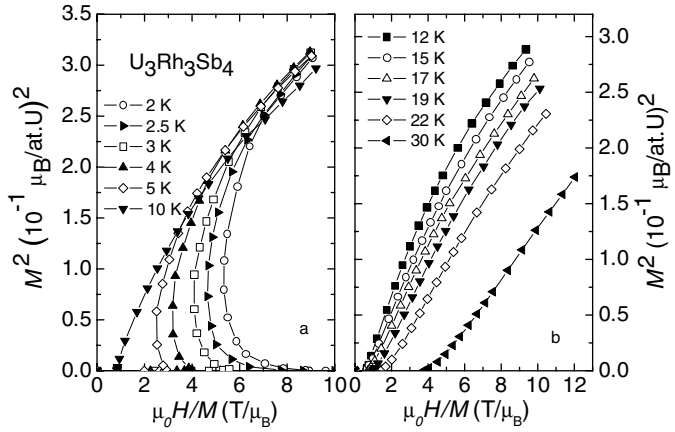

Figure 7. The M^2 versus H/M plots for the isotherms at several temperatures between (a) 2 and 10 K, and (b) 12 and 30 K.

In order to gain insight into the nature of the magnetic ground state of the studied compound, the isotherm data were analysed with the help of the Arrott plot. As can be seen in figure 7(a), the isotherms at low fields show a drastic change with temperature, i.e., there is a change in the sign of the slope of the M^2–H/M function, from a negative slope for $T \leqslant 5$ K to a positive one at 10 K. For the magnetization curves at temperatures up to 5 K the sign of the slope changes also with increasing field strength and consequently at fields larger than 1 T the positive slope is noticed. One important thing should be noted here: that the extrapolation of the M^2–H/M curves for data at fields larger than 3.5 T to $H \to 0$ with a positive intercept seems to be possible. For example, at 2 K such a extrapolated magnetization is about 0.3 μ_B. This fact may indicate that in low fields some antiferromagnetic correlations dominate, but in higher fields the ferromagnetic ones become induced.

In figure 7(b) we show the Arrott plot for the magnetization taken at several temperatures between 12 and 30 K. In the simple mean field case, the M^2 versus H/M dependence at

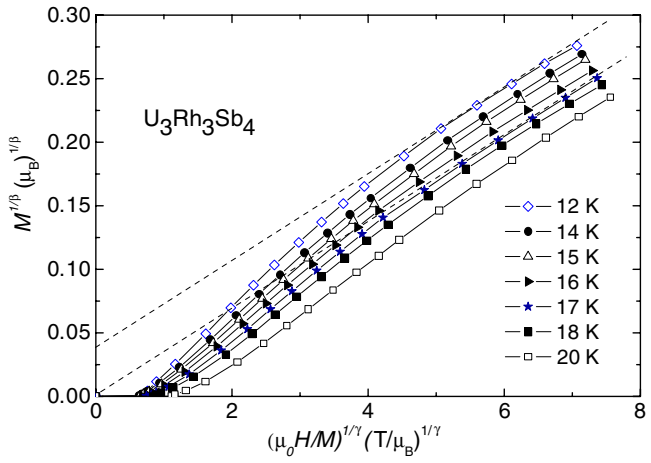

Figure 8. Modified Arrott plots of isotherms for temperatures near T_C. The dashed lines illustrate the validity of the modified Arrott plots above 3 T.

various temperatures should show a series of parallel lines in accordance with the magnetic equation of state of the form $M^2 = A + B * H/M$. For ferromagnets, the coefficient $A > 0$ in the ordered state, but $A < 0$ in the paramagnetic state and $A = 0$ at the Curie temperature. For $U_3Rh_3Sb_4$, however, some deviation from linearity is clearly seen in these isotherms. Nevertheless, according to Arrott and Noakes [23], one improves the linearity of the isotherms by varying the critical exponents β and γ in the equation

$$H/M^{1/\gamma} = \frac{T - T_C}{T_1} + \left(\frac{M}{M_1}\right)^{1/\beta}. \tag{2}$$

Such an expression does contain the information on spontaneous magnetization σ_s below T_C

$$\sigma_s \sim (T_C - T)^{\beta} \tag{3}$$

and the inverse susceptibility just above T_C

$$\chi^{-1} \sim (T - T_C)^{\gamma}, \tag{4}$$

where T_1 and M_1 are constants. The fitting of the experimental data to equation (2) yields $\beta = 0.483(4)$, $\gamma = 1.14(2)$ and $T_C = 16.8(3)$. Based on these parameters the modified Arrott plots (figure 8) can be constructed. The isotherms are now straight lines at fields above 3 T that could prove the validity of the choice of β and γ. From figure 8 we have derived the spontaneous magnetization and the zero-field susceptibility, which are shown in figure 9 as a function of temperature. This figure somewhat justifies the application of equations (3) and (4) and allows us to evaluate the average value of the Curie temperature to be of 17.3(2) K. Bearing in mind the fact that both σ_s and χ^{-1} are the extrapolated values for $H \to 0$ and no sign of the spontaneous magnetization can be detected at fields below 3 T, one may suspect that the magnetic phase transition at T_C is a magnetic field induced transition and in reality there is no ferromagnetic transition at zero field.

3.4. Electronic transport properties

In figure 10 we show the temperature dependence of the electrical resistivity (a) and thermoelectric power (b). Qualitatively, the resistivity of $U_3Rh_3Sb_4$ is similar to that of

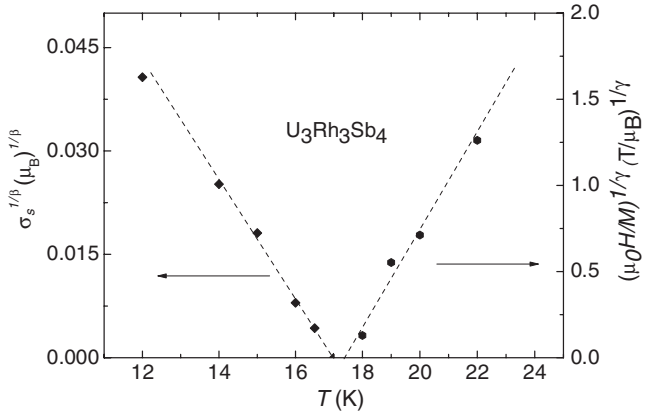

Figure 9. Temperature dependence of spontaneous magnetization and zero-field susceptibility derived by the modified Arrott plots. The dashed lines are guides for the eye.

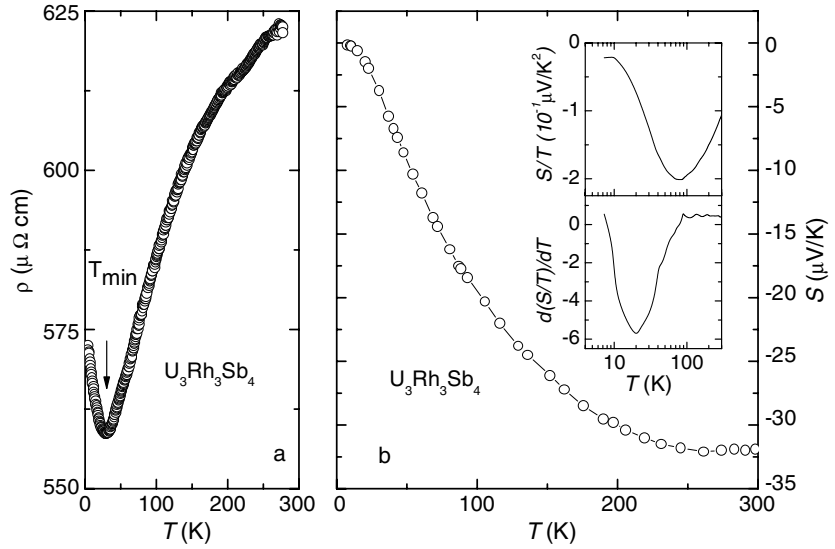

Figure 10. Temperature dependences of (a) electrical resistivity and (b) thermoelectric power. The upper inset shows the temperature derivative of the modulus of the ratio S/T. The lower inset gives the temperature derivative of S/T in arbitrary units as a function of temperature.

$U_3Cu_3M_4$ (M = Sn and Sb) [4]. For these compounds, a weak temperature dependence of the resistivity and a large value at room temperature, ρ_{RT}, were observed. For $U_3Rh_3Sb_4$ we have estimated the ratio $\rho_{300\ K}/\rho_{4\ K}$ to be 1.1 and ρ_{RT} about 600 (100) $\mu\Omega$ cm. This large value may point out some atomic disorder in the sample, though this effect is not seen by the x-ray diffraction analysis. This could be explained by the fact that the x-ray method may detect a disorder on the level of a few per cent and the resistivity may reflect the disorder on the micro-scale level. The large error given for the resistivity was due to uncertainty about the sample dimension. An interesting finding in $U_3Rh_3Sb_4$ is the observation of a minimum in $\rho(T)$ at 30 K and an upturn in the resistivity below this temperature observed down to 4 K. Because this anomaly cannot be associated with any characteristic temperatures, one

has to exclude at the moment any magnetic mechanism causing such a behaviour. However, one may invoke another mechanism to explain this upturn in the resistivity, for instance, a Kondo-type effect [24]. However, the low temperature resistivity of $U_3Rh_3Sb_4$ does not show the logarithmic behaviour characteristic of a Kondo effect, but rather follows a $T^{1/2}$ dependence (not shown here). In turn, this dependence is very familiar with an electron localization effect [25–27]. Alternatively, this resistivity minimum may also be associated with the development of short-range antiferromagnetic correlation, as in the case of U_2PtGa_3 [28]. Such correlations have also been found in a number of other concentrated f-electron spin glasses, for instance in U_2PdSi_3 [29] and U_2RhSi_3 [30].

The absolute thermopower, shown in figure 10(b) is found to be negative over the entire temperature range. At room temperature S reaches a considerable high value of $-32\ \mu V\ K^{-1}$, i.e., one order of the magnitude larger than that in ordinary metals. Relatively large values of both S and ρ are consistent with the behaviour of a low charge carrier system. It is well known that the thermoelectric power of materials consists of many contributions having different origins. For instance, in ordinary metals, there are at least two contributions to the total thermopower, diffusion S_d and phonon drag S_g contributions. For magnetic materials, one should also take into account other magnetic contributions, e.g., magnon drag, which may appear below the magnetic phase transition. In the case of $U_3Rh_3Sb_4$, the S_g component seems to be minor, since we do not observe any maximum in $S(T)$ at low temperatures, which could support the phonon drag process. On the other hand, S_d according to the Mott formula [31]

$$S = -\frac{\pi^2}{3}\frac{k_B^2 T}{e\sigma(E_F)}\frac{d\sigma(E_F)}{dE} \tag{5}$$

depends on both the electrical conductivity at the Fermi level, $\sigma(E)$, and its energy derivative, $\frac{d\sigma(E_F)}{dE}$. In equation (5) k_B is the Boltzmann constant and e is the elementary charge. When plotting the temperature dependence of the S/T ratio, which approximately represents the temperature dependence of the resistivity, we see that below 79 K this ratio starts to increase (see the upper inset of figure 10(b)), qualitatively explaining the behaviour of the resistivity. In the lower inset of figure 10(b) we have plotted the temperature derivative $d(S/T)/dT$ versus T in order to get any information of the influence of any change at the Fermi surface on the thermopower. Consequently, just near T_C a maximum in this derivative appears. This feature may suggest that the occurrence of the ferromagnetic correlation drives some change at the Fermi surface.

4. Discussion and conclusions

The complex double-transition behaviour of $U_3Rh_3Sb_4$ (paramagnetic-induced ferromagnetic spin glass) is puzzling, and therefore this needs further studies. We may consider some circumstances for the appearance of the spin-glass behaviour in $U_3Rh_3Sb_4$. In classical manner, each of the factors such as spin frustration and disorder need to be taken into account. Although the crystal structure of $U_3Rh_3Sb_4$ is an ordered one, we cannot, however, exclude any crystallographic disorder at all. From the crystallographic point of view, it is possible for the spin frustration phenomenon to occur. Actually, in the noncentrosymmetric $Y_3Au_3Sb_4$-type crystal structure the uranium atoms occupying the crystallographic positions 12(a) belong to two/three different uranium sublattices. This means that each uranium sublattice can have different values of magnetic moments which are able to orientate independently to one another. Thus, in spite of the cubic symmetry of the crystal, the local symmetry of the uranium ions, in fact, is a tetragonal one and such an atomic arrangement can lead to a remarkable

uniaxial anisotropy. In addition, an indirect exchange between magnetic ions seems to be significant since the U–U distance in this compounds (4.4 Å) is much larger than the Hill limit (3.5 Å), where the direct f orbital has physical significance. Thus, we are supposing that the coexistence of the indirect exchange interactions and the uniaxial anisotropy stand for the spin frustration and this in turn drives the spin-glass phenomenon in $U_3Rh_3Sb_4$ at low temperatures. The frustration has already been demonstrated in some examples of the U_3X_4 compounds crystallizing in the unfilled Th_3P_4-type structure (the uranium sublattices are at the same positions as those in the filled $Y_3Au_3Sb_4$-type structure). For example, the spin frustration leads these compounds to have different magnitudes of the magnetic moments in their collinear structures [32–34]. At this point we should mention that the isostructural compound $Ce_3Cu_3Sb_4$ shows a canted antiferromagnetic structure [35].

In conclusion, we have grown a set of small single crystals of $U_3Rh_3Sb_4$ by means of the In-flux method. Based on single-crystal x-ray diffraction data we have refined the crystal structure to be of the cubic $Y_3Au_3Sb_4$ type, isostructural with the stannides $U_3T_3Sn_4$ and antimonides $U_3T_3Sb_4$, reported earlier in the literature. The magnetization and ac-susceptibility data show that $U_3Rh_3Sb_4$ has a spin-glass ground state. We believe that the mechanism leading to this state is a competition between magnetic exchange interactions and uniaxial anisotropy; these provide a mixture containing some ratio of the ferromagnetic and antiferromagnetic uranium sublattices. The development of antiferromagnetic correlations at low temperatures probably locks up some ferromagnetic clusters, from which the spin-glass state is formed. We suggest a ferromagnetic phase transition induced by magnetic field at about 17 K. We have analysed the critical magnetic behaviour of $U_3Rh_3Sb_4$ at temperatures near T_C. The observed values of critical exponents β and γ are closer to the mean-field values than to the Heisenberg ones. The electron transport properties suggest that $U_3Rh_3Sb_4$ can be classified as a low carrier system.

References

[1] Dwight A E 1979 *J. Nucl. Mater.* **79** 417
[2] Buschow K H J, de Mooij D B, Palstra T T M, Niewenhuys G J and Mydosh J A 1985 *Philips J. Res.* **40** 313
[3] Takabatake T, Miyta S, Fujii H, Aoki Y, Suzuki T and Fujita T 1990 *Physica* B **165/166** 437
[4] Takabatake T, Miyta S, Fujii H, Aoki Y, Suzuki T, Fujita T, Sakurai J and Hiraoka T 1990 *J. Phys. Soc. Japan* **59** 4412
[5] Canfield P C, Thompson J D, Fisk Z, Hundley M F and Lacerda A 1992 *J. Magn. Magn. Mater.* **108** 217
[6] Sanchez-Castro C 1996 *Phil. Mag.* B **73** 525 and references therein
[7] Endstra T, Niewenhuys G J, Mydosh J A and Buschow K H J 1990 *J. Magn. Magn. Mater.* **89** L273
[8] Sechovsky V and Havela L 1998 *Handbook of Magnetic Materials* vol 11, ed K H J Buschow (Amsterdam: Elsevier Science B V) chapter 1, p 200 (Ref. Endstra 1992)
[9] Henkie Z, Maślanka R, Oleksy Cz, Przystawa J, de Boer F R and Franse J J M 1987 *J. Magn. Magn. Mater.* **68** 54
[10] Oleksy Cz 1984 *Acta Phys. Pol.* A **66** 665
[11] Canfield P C and Fisk Z 1992 *Phil. Mag.* B **65** 1117
[12] Sheldrick G M 1997 *SHELXL-97, Program for crystal structure refinement and SHELXS-97* University of Göttingen, Germany
[13] Mulder C A M, van Duyneveldt A J and Mydosh J A 1982 *Phys. Rev.* B **25** 515
[14] Goldfarb R B, Fickett F R, Rao K V and Chen H S 1982 *J. Appl. Phys.* **53** 7687
[15] Mydosh J A 1993 *Spin Glasses: An Experimental Introduction* (London: Taylor and Francis)
[16] Ferré J, Rajchenbach J and Malletta H 1981 *J. Appl. Phys.* **52** 1697
[17] Tholence J L 1980 *Solid State Commun.* **35** 113
[18] Zhao J H, Kunkel H P, Zhou X Z, Williams G and Subramanian M A 1999 *Phys. Rev. Lett.* **83** 219
[19] Ma S K 1976 *Modern Theory of Critical Phenomena* (New York: Benjamin)
[20] de Almeida J R L and Thouless D J 1974 *Phys. Rev. Lett.* **32** 1792
[21] Barbara B, Malozemoff A P and Imry Y 1981 *Physica* B **108** 1289
Barbara B, Malozemoff A P and Imry Y 1981 *Phys. Rev. Lett.* **47** 1852

[22] Ohama T, Yasuoka H, Takabatake T and Fujii H 1993 *Japan. J. Appl. Phys.* **8** 215
[23] Arrott A and Noakes J E 1967 *Phys. Rev. Lett.* **19** 786
[24] Kondo J 1964 *Prog. Theor. Phys.* **32** 37
[25] Abrahams E, Anderson P W, Licciardello D C and Ramakrishnan T V 1979 *Phys. Rev. Lett.* **42** 673
[26] Alt'shuler B L and Aronov A G 1985 *Electron–Electron Interactions in Disordered Systems* vol 1, ed A L Efros and M Pollack (Amsterdam: North-Holland)
[27] Lee P A and Ramakrishnan T V 1985 *Rev. Mod. Phys.* **57** 287
[28] Tran V H, Steglich F and André G 2002 *Phys. Rev.* B **65** 134401
[29] Li D X, Shiokawa Y, Homma Y, Uesawa A, Dönni A, Suzuki T, Haga Y, Yamamoto E, Honma T and Ōnuki Y 1998 *Phys. Rev.* B **57** 7434
[30] Li D X, Dönni A, Kimura Y, Shiokawa Y, Homma Y, Haga Y, Yamamoto E, Honma T and Ōnuki Y 1999 *J. Phys.: Condens. Matter* **11** 8263
[31] Mott N F and Davis E A 1979 *Electronic Processes in Non-Crystalline Material* (Oxford: Oxford University Press) p 52
[32] Burlet P, Rossat-Mignod J, Troć R and Henkie Z 1981 *Solid State Commun.* **39** 745
[33] Wiśniewski P, Gukasov A and Henkie Z 1999 *Phys. Rev.* B **60** 6242
[34] Sandratskii L M and Kübler J 1997 *Phys. Rev.* B **55** 11395
[35] Herrmannsdörfer T, Fischer P, Wachter P, Wetzel G and Mattenberger K 1999 *Solid State Commun.* **112** 135